ARTICLE

Co-Revolving Topological Defects in a Nematic Liquid Crystal

Adam L. Susser^a, Samo Kralj^b, and Charles Rosenblatt^a

Received 00th January 20xx, Accepted 00th January 20xx

DOI: 10.1039/x0xx00000x

A patterned surface defect of strength m=+1 and its associated disclination lines can decompose into a pair of surface defects and disclination lines of strength m=+1. For a negative dielectric anisotropy liquid crystal subjected to an applied ac electric field E, these half-integer defects are observed to wobble azimuthally for E > than some threshold field and, for sufficiently large fields, to co-revolve antipodally around a central point approximately midway between the two defects. This behavior is elucidated experimentally as a function of applied field strength E and frequency V, where the threshold field for full co-revolution scales as $V^{1/2}$. Concurrently, nematic electrohydrodynamic instabilities were investigated. A complete field Vs. frequency "phase diagram" compellingly suggests that the induced fluctuations and eventual corevolutions of the ordinarily static defects are coupled strongly to — and driven by — the presence of the hydrodynamic instability. The observed behaviour suggests a Lehmann-like mechanism that drives the co-revolution.

1 Introduction

Topological defects (TDs) can be found throughout nature on length scales spanning more than 30 orders of magnitude¹⁻⁵. Many of these defects are rendered inaccessible for direct study due to their often vast or minute size and time scales. However, the convenient length scales and large mechanical and optical anisotropies of liquid crystals (LCs) long have made LCs an ideal system for the visualization and investigation of TDs⁶⁻¹⁰.

In a recent paper we examined two scenarios 11 : i) a negative dielectric anisotropy ($\Delta \varepsilon < 0$) nematic LC for which an electric field converts an escaped radial defect of surface strength m=+1 into a pair of m=+12 surface defects and their associated disclination lines that traverse the cell, and ii) the reverse process of a field-driven merger of two m=+12 defects into an m=+1 surface defect when $\Delta \varepsilon > 0$. We had noted a novel phenomenon for the first case ($\Delta \varepsilon < 0$), viz., the appearance of an azimuthal co-revolution of the two half-integer defects around a common central point when the applied ac electric field exceeds a frequency-dependent threshold value. [In our previous work 11 we referred to this behaviour as "co-rotation". We believe that "co-revolution" is a more accurate description, and have adopted this terminology throughout this paper.]

Consider a radial m = +1 patterned surface defect and its associated disclination line. This disclination line connects the patterned "master" surface and the opposing planar

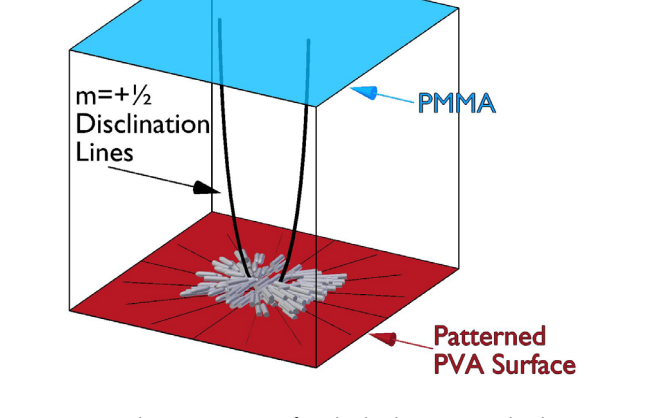


Fig. 1 Cartoon showing a master surface that has been patterned with an m=+1 defect using an atomic force microscope, and an opposing substrate treated for planar degenerate alignment. In this image, the m=+1 escaped radial defect has split into two daughter $m=+\frac{1}{2}$ surface defects, with disclination lines reaching the top planar degenerate surface.

degenerate surface and may have an escaped radial director

configuration. The liquid crystal has a negative dielectric anisotropy. On application on an ac electric field E perpendicular to the substrates (along the z-axis), the escaped director field is driven toward the xy-plane. To reduce the overall energy cost, the m=+1 defect can decompose into a pair of $m=+\frac{1}{2}$ defects with two disclination lines running between the substrates (Fig. 1). In light of theoretical calculations by Chiccoli, et al¹², we examined this phenomenon in detail¹¹, reporting on the critical field required for the conversion from a single escaped radial TD to a pair of split defects. Once split, the two half-integer defects were found to remain decomposed even as the field is brought back to zero. On again increasing the field, we reported that at some threshold field the two

Electronic Supplementary Information (ESI) available: Videos of the co-revolving defects. See DOI: 10.1039/x0xx00000x

a. Department of Physics, Case Western Reserve University, Cleveland, Ohio 44106 USA

b. Department of Physics, Faculty of Natural Sciences and Mathematics, University of Maribor, Koroška cesta 160, SI-2000 Maribor, Slovenia and Jožef Stefan Institute, P.O. Box 3000, SI-1000 Ljubljana, Slovenia

defects begin to co-revolve around a central point, that is, around the core of the patterned $m=\pm 1$ defect. It is important to note that the master surface patterning serves two roles: It establishes the director pattern at this surface and also approximately pins in place the surface defect. That is, the two half-integer defects are confined to a region very close (of order 2 μ m) to the core of the patterned integer defects. We want to emphasize that the co-revolution phenomenon also can be observed for a pair of closely-spaced, initially $m=\pm 1/2$ defects, without the need to decompose an originally $m=\pm 1/2$ defect into a pair of half-integer defects.

In this paper we focus on an experimental investigation, primarily by optical microscopy, of the co-revolution process. In particular, we examine pre-co-revolution azimuthal "wobbling" of what are ordinarily static TDs as a function of applied field strength $\it E$ and frequency $\it v$, as well as the onset and behaviour in the fully co-revolving regime, including the angular velocity ω vs. both $\it E$ and $\it v$ of the co-revolving TDs. We also examine the behaviour of an observed electrohydrodynamic (EHD) instability — eponymously called the Carr-Helfrich instability¹³⁻ ¹⁶ after those who explained the basic behaviour — associated with the nematic LC's negative dielectric anisotropy and positive electrical conductivity anisotropy. We find that the associated threshold fields are close in value to those for defect wobble. The data suggest that the two phenomena are linked, with the moving EHD domains inducing an angular velocity of the defect pair. This supposed connection is made stronger by the absence of co-revolution behaviour for a pair of $m = +\frac{1}{2}$ defects in a positive dielectric anisotropy LC, where the EHD instability does not occur. Moreover, we believe that the EHD instability provides the conditions to trigger an electric Lehmann-like effect^{17,18}, which could explain the rotational dynamics of the $m = +\frac{1}{2}$ defects. We note that all measurements are at frequencies ν corresponding to the dielectric regime of the EHD instability, and therefore we discuss the phenomena in terms of electric fields rather than voltages.

2 Experimental

The cell was constructed using semi-transparent indium-tinoxide (ITO) coated glass slides; the ITO was used for application of an electric field across the cell. One slide was spin-coated with the polymer polyvinyl alcohol (PVA, $M_w = 31000 - 50000$) and baked at 120°C for 120 min. The PVA then was scribed using the stylus of an atomic force microscope with a patterned 3 x 3 array of alternating m = +1 and -1 defects, with variable scribed line spacing ~ 100 to 300 nm, depending on the local curvature; this corresponds to the patterned "master" surface. Details of the scribing procedure can be found in Ref. 19. The opposing substrate was spin-coated with a thin layer of the planar degenerate alignment material polymethyl methacrylate (PMMA)²⁰, which was diluted in a 2:1 volume ratio mixture of propylene glycol methyl ether acetate (PGMEA) and γ butyrolactone to a concentration of 13 wt-%. After drop-casting the PMMA solution, the substrate was spun for 40 s at 2600 rpm, and then baked at 80°C for 120 min. A cell was constructed by placing the substrates together, separated by Mylar spacers,

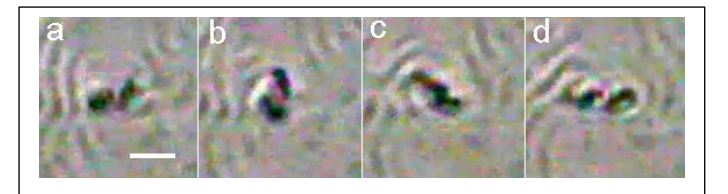


Fig. 2 Electrohydrodynamic instability and concomitant counter-clockwise revolution of defect pair at $E=6.5~\rm V~m^{-1}$ and $v=250~\rm Hz$. Approximately 1/15 s (2 video frames) separates successive images. Scale bar corresponds to 10 μm .

and cementing. The thickness h of the cell was found to be h = $10.85 \pm 0.06 \, \mu m$ as determined by optical interferometry. Our experiments focused on one of the m = +1 patterned surface defects.

The cell was filled by capillary action in the isotropic phase with the negative dielectric anisotropy mixture liquid crystal ZLI-4330 (Merck). It was then cooled slowly to room temperature, where it exhibits a nematic phase of dielectric anisotropy $\Delta \epsilon$ = -1.9 and optical birefringence $\Delta n = 0.15$ [manufacturer's specifications]. An electric field at four different frequencies (ν = 125, 250, 500, and 1000 Hz) was applied across the cell, and observations using transmission optical microscopy (unpolarised) with a 50x objective were recorded in the following manner: At a given frequency v, a range of electric fields was selected such that the minimum field was below all thresholds of interest and the maximum was at a point where the defects moved highly chaotically. A video was recorded at a rate of 30 frames s-1 at 2.07 megapixels per frame as the field was stepped up every 10 s, with the step size being 1/58th of the full field range. The entire process was repeated at the three other frequencies.

3 Experimental Results and Discussion

We first consider the defects and their motion. The defects were found to be completely immobile below a frequency-dependent threshold field E_{rev1} , where E_{rev1} increases monotonically with increasing frequency v. (Videos of the behaviours discussed in this paragraph can be found in the Electronic Supplementary Information online.) Above E_{rev1} the antipodal defects were found to regularly fluctuate azimuthally along partial arcs about their shared center. This behaviour, which corresponds to the "wobble" mentioned above, had not been discussed in Ref. 11 but had been observed during those experiments. On further increasing the electric field, a second frequency-dependent threshold field E_{rev2} was observed, above which the antipodal defects would switch irregularly between wobble and both full (360°) and half (180°) co-revolution. At a still higher third threshold field E_{rev3} , full co-revolution (without intervals of wobble) was the only behaviour observed.

A series of images depicting the co-revolution as a function of time is shown in Fig. 2. Note that in Ref. 11 the critical field E_c for full revolution, which corresponds to E_{rev3} in this work, was found to vary approximately as $v^{1/2}$ over the frequency range $500 \le v \le 4000$ Hz; the same holds true herein, in which $E_{rev3} \propto v^{1/2}$ over the frequency range $125 \le v \le 1000$ Hz, with a correlation coefficient $R^2 = 0.992$. In this work all three threshold fields were found to increase

Journal Name ARTICLE

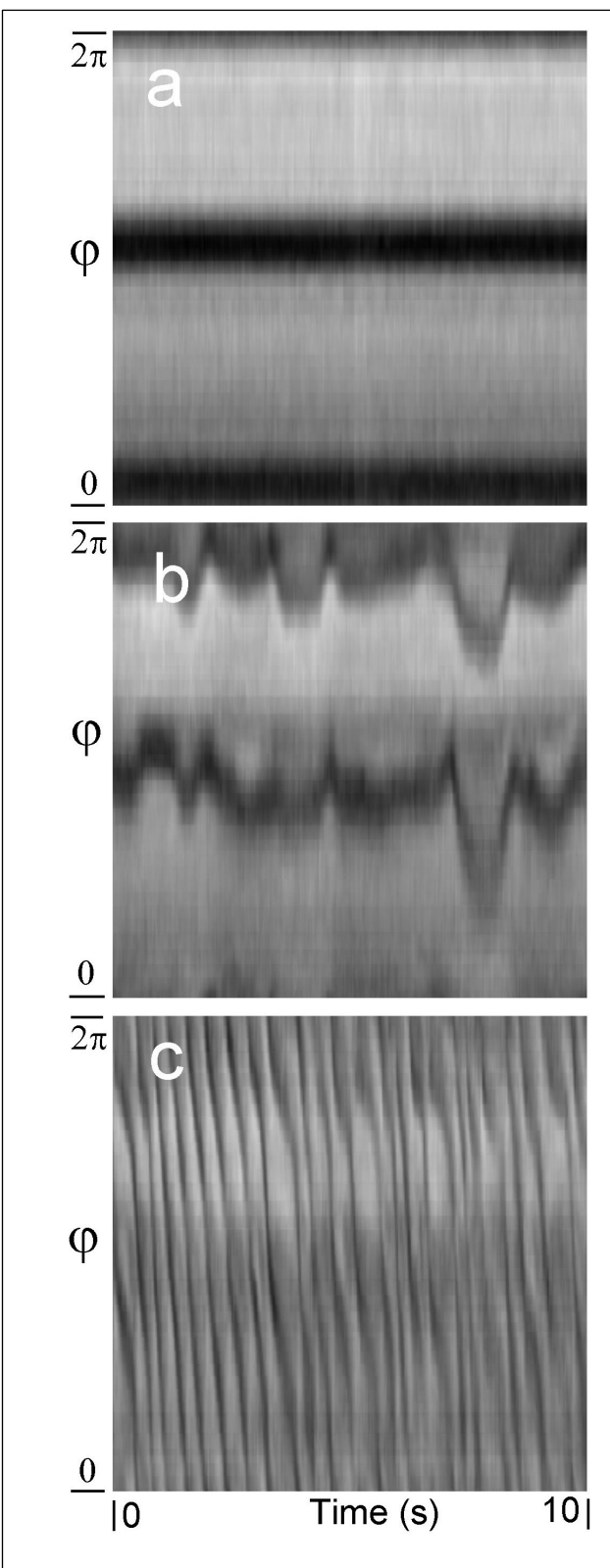
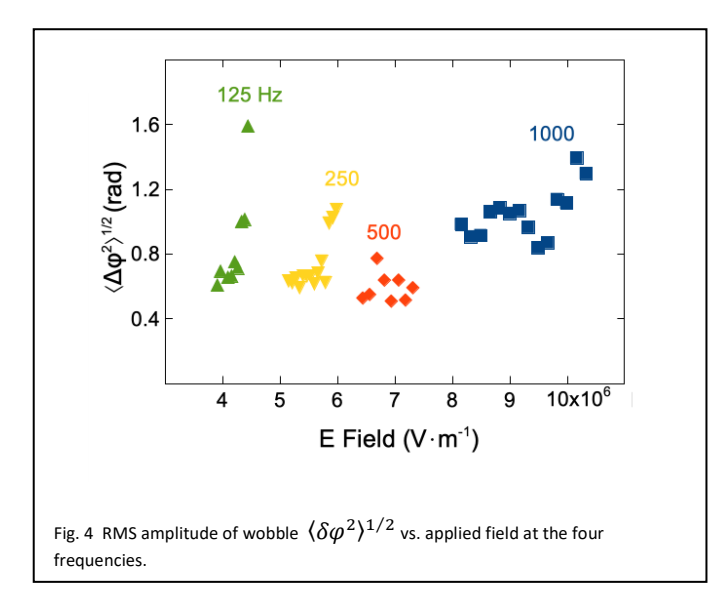


Fig. 3 Azimuthal coordinate ϕ (vertical axis) at time t (horizontal axis). Each pixel corresponds to the average intensity of light along the radial line $1.11 < r_o < 3.71$ μ m, where the half-integer defects can pass through this region. a) Low field $E < E_{rev1}$ in which the defects are fixed in position. b) The defect wobble regime in which $E_{rev1} < E < E_{rev2}$. c) The co-revolution regime $E > E_{rev3}$. Displayed images are at driving frequency v = 250 Hz. See text for detailed explanation.

monotonically with frequency. Moreover, $E_{rev3} - E_{rev2}$ is negligible at v = 125 Hz, but grows monotonically with increasing frequency. Figure 2 shows counter-clockwise revolution. We find that the sense of revolution for a given defect pair is fixed, even if the field is reduced to zero and subsequently increased, as well as on heating and then recooling through the nematic-isotropic phase transition. However, a given defect pair may co-revolve either clockwise or counter-clockwise, even when nearby defect pairs in the same cell revolve in opposite senses. This suggests that the sense of rotation is determined by symmetry-breaking imperfections in the initial surface patterning.

Figure 3 shows a representative analysis of the data for the TDs at frequency v = 250 Hz, with the image analysis performed using ImageJ® software. In all three panels, at a given frequency v and a given electric field amplitude E, the horizontal axis corresponds to time t, with t = 0 at the left and t = 10 s at the right. The vertical axis corresponds to the azimuthal coordinate ϕ of the defects and runs from φ = 0 at the at the bottom of each panel to φ = 2π at the top. The brightness of each pixel corresponds to the average light intensity detected along the radial line 1.11 < r_0 < 3.71 μm at azimuthal coordinate φ at time t. Thus, in Fig. 3a, which corresponds to a weak applied field $E = 3.46 \ V \ m^{-1} < E_{rev1}$ (and thus stationary behaviour), the intensity is constant at a given azimuthal angle ϕ during the entire 10 seconds over which this field was applied. This representation indicates that the defects were fixed in position, with the two dark horizontal bars corresponding to approximately antipodal defects an angle $\Delta \phi \approx \pi$ apart.

Figure 3b corresponds to a field $E_{rev1} < E < E_{rev2}$, where $E=5.72~\rm V~m^{-1}$, that is, in the regime in which the antipodal defects wobble azimuthally about the central point. For example, looking at the jagged dark region that runs from left to right across the center of the figure at approximately $\phi=\pi$, as one moves from the left side of the figure (t=0) to the right side $(t=10~\rm s)$ it is apparent that this defect undergoes azimuthal wobble over time. Moreover, the lateral extent of the dark region allows us to extract both the rms amplitude $(\delta \varphi^2)^{1/2}$ and approximate period P_{wob} of the wobble. The former is shown in Fig. 4 for all four frequencies as a function of applied field, and the latter in shown as *inverse* period $1/P_{wob}$ in Fig. 5 at three frequencies. (The wobble becomes too irregular at $v=1000~\rm Hz$ to



extract P_{wob} .) We remark that the rms amplitude of the wobbling tends to increase with applied field for at least three of the four frequencies. (Note that what appears to be a piece of dust had become trapped in the defects and rendering these data at v = 500 Hz only partially reliable.) In particular, at the lowest frequency v = 125 Hz, the rms amplitude appears to grow especially rapidly with field as E approached E_{rev2} .

The next field regime $E_{rev2} < E < E_{rev3}$ corresponds to a highly irregular variation between wobble and half and full co-revolution behaviours. (This is not shown in Fig. 3.) Here wobble occurs for a

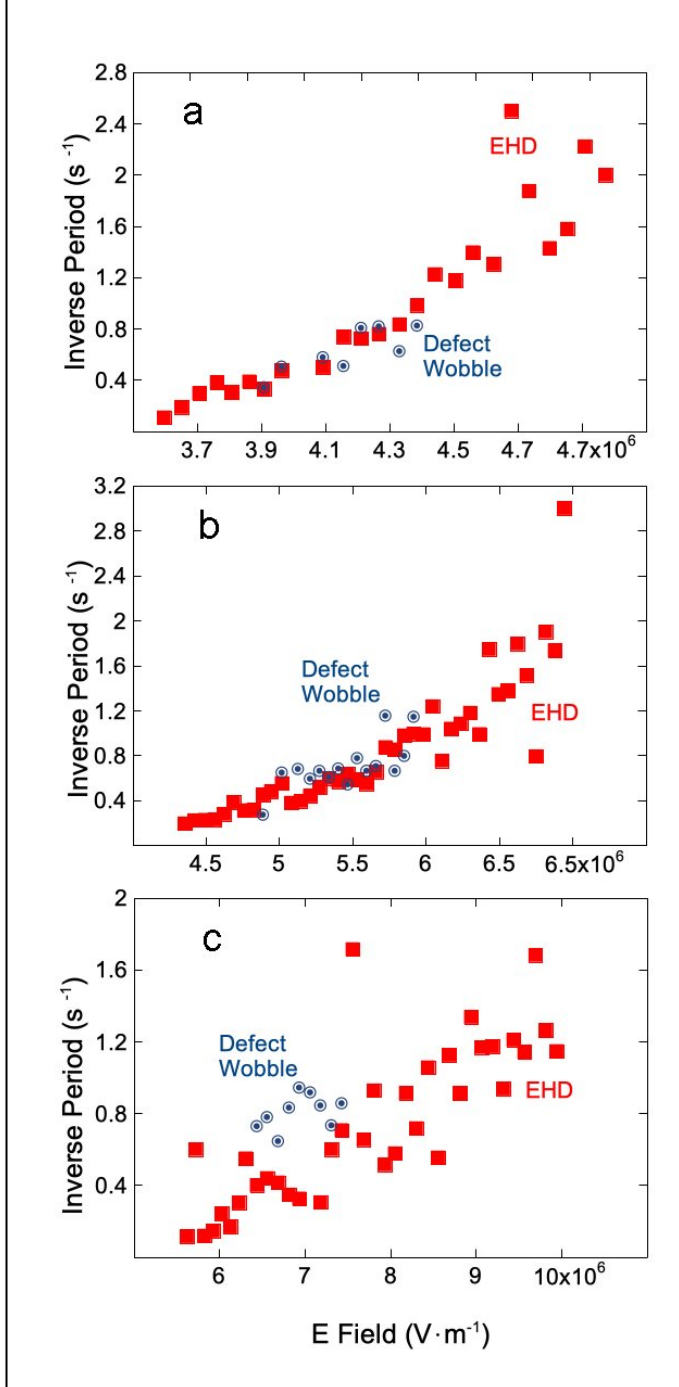


Fig. 5 Wobble inverse temporal period P_{wob} -1 (blue bull's eye circles) and inverse temporal period of EHD instability P_{EHD} -1 (red squares) vs. applied field at v = 125 (a), 250 (b), and 500 Hz (c).

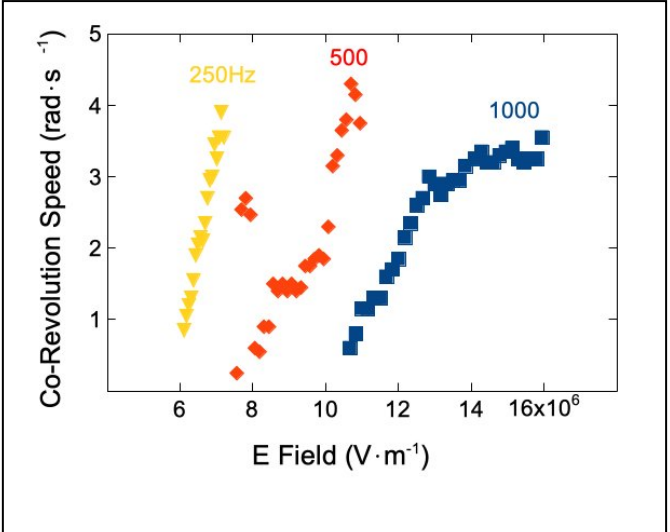


Fig. 6 Angular velocity of co-revolving defects vs. applied field for three different driving frequencies: yellow triangles for ν = 250 Hz, orange diamonds for 500 Hz, and blue squares for 1000 Hz.

few seconds, followed by one or more half or full co-revolutions, followed again by a brief period of wobble. The *range* of field $\Delta E_{rev32} = E_{rev3} - E_{rev2}$ for this behaviour is rather small, virtually negligible at 125 Hz and increasing monotonically to ΔE_{rev32} =1.17 V m⁻¹ (or approximately 12% of E_{rev2}) at 1000 Hz. (In voltage, $V_{rev2} - V_{rev1} = 120$ V - 107 V = 13 V).

Finally, for E (= 6.24 V m⁻¹) > E_{rev3} , only full co-revolution is observed. Figure 3c shows this behaviour as a series of dark and light slanted stripes. As in Figs. 3a and 3b, the dark regions correspond to the half-integer defects. With increasing time, the defects co-revolve around their common central point, and thus their azimuthal angle changes continuously with time. The slope of the dark stripes, $d\phi/dt$, corresponds to the angular velocity ω of the defects. Thus the horizontal dark stripes in Fig. 3a indicate zero angular velocity, whereas the nearly vertical stripes in Fig. 3c correspond to a large value of ω . These are shown in Fig. 6. Importantly, we note that the angular velocity may not be constant at a fixed field, a behaviour reflected in a change of slope of the dark stripes in Fig. 3c. Occasionally the angular velocity may change nearly discontinuously for a short period, which apparently occurs as a piece of dust moves through. Figure 6 indicates that although the angular velocity does not depend strongly on the driving frequency, the fields required to induce co-revolution increase with increasing driving frequency.

We believe that the co-revolution of TDs arises from an extension of the Carr-Helfrich EHD instability¹³⁻¹⁵ into the higher frequency regime. Such an instability induces both ion flow associated with the traveling domains and chirality, allowing for electric Lehmann-like rotation^{17,18}. In the following we describe the relevant EHD regime and analyse why an electric Lehmann-like effect¹⁷ is a good candidate to explain the co-revolution.

The Carr-Helfrich EHD instability is well known in LCs possessing a negative dielectric anisotropy and positive conductivity anisotropy¹³⁻¹⁵. In the presence of a director distortion and in light of the positive conductivity anisotropy, the

Journal Name ARTICLE

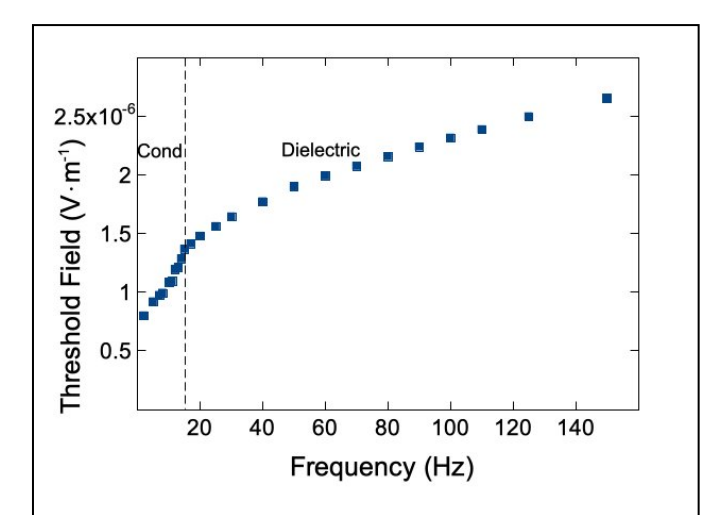


Fig. 7 Threshold of EHD instability vs. driving frequency. The low frequency range (v < 20 Hz) corresponds to the conduction regime; the dielectric regime corresponds to v > 20 Hz. This result shows that experiments reported herein were performed in the dielectric regime.

applied electric field causes a spatially varying build-up of charge. This in turn exerts an electrostatic torque on the negative dielectric anisotropy director, which has the effect of increasing the initial director distortion. Ultimately, the total electric field causes material flow, resulting in a hydrodynamic torque, furthering the positive feedback on the director distortion. These torques compete with the elastic restoring torque, resulting in a critical field below which the LC director is stable but above which quasi-periodic stripes appear. At low frequencies v, also known as the conduction regime, the critical fields — actually critical voltages for this frequency regime tend to be small, whereas the critical fields at higher frequencies, also known as the dielectric regime, tend to be much larger. Because of the relatively large conductivity of a material like MBBA (methoxybezylidene butylanailine) the crossover frequency ν_c between the two regimes typically lies around 100 Hz²¹; for lower conductivity materials such as ZLI-4330 used in our experiments, this crossover regime is lower. Figure 7 shows the electric field vs. frequency curve obtained far from the TDs for the onset of this hydrodynamic instability. We see that ν_c for ZLI-4330 is approximately 20 Hz, indicative of a low conductivity material. Importantly, this means that all our measurements of the corevolving defects occur at frequencies associated with the EHD instability dielectric regime. In this regime it is the electric fields rather than the applied voltages that characterize the onset of various behaviours, and it is for this reason that we express the electric phenomena in terms for fields rather than voltages.

The classical Lehmann effect¹⁷ describes the rotation of cholesteric droplets within a plane-parallel cell subjected to a temperature gradient along the cell thickness. In that case, the key ingredients that enable the rotation are chirality and thermal flow. In our setting we propose that the co-revolution of TDs is due to behaviours that arise from the EHD instability, ¹³⁻¹⁵ which is instrumental in inducing both chirality and charge flow to create an electric Lehmann-like effect ^{17,18}. This mechanism triggers flow in the

physical fields that describe our system. We suggest that the resulting EHD traveling domains, which produce curvature lines that are attractors for electrical charge, give rise to synchronized ion movement. This, along with the related mechanical stress field, can serve as an analogue for thermal flow. With the addition of chiral symmetry breaking (discussed below), Lehmann-like behaviour may ensue.

It is important to note that molecular-level chirality is not a required ingredient for the Lehmann-type phenomena. Namely, such effects are also observed in LC director fields exhibiting sufficiently low symmetries 18,22. This allows the onset of effective global chirality – here a twist deformation – in the presence of an appropriate symmetry breaking generator. In our case, a local twist preference could be enabled by the EHD wave instability. Namely, our analysis shows that the |m| = 1/2 director profile superimposed on a simple EHD harmonic wave yields a finite twist elastic deformation. In our estimate we use the parametrization $\vec{n}=$ $(cos\theta cos\phi, cos\theta sin\phi, sin\theta)$ in the Cartesian coordinates (x,y,z). In the absence of the EHD instability, a straight (i.e., linear) $m=\pm 1/2$ disclination, centered at (x=0, y=0), obtains in the approximation of equal Frank elastic constants⁶ described by $\phi = m \operatorname{ArcTan}\left(\frac{y}{x}\right)$ and heta=0. In this case twist elastic deformation is absent. We then mimic the presence of an EHD excitation by a simple traveling harmonic wave $\theta = \theta_0 \cos(\vec{k} \cdot \vec{r} - \omega t)$, traveling, say, along the x-axis. The resulting twist deformation in this case is non-zero. (In the lowest approximation: $\vec{n} \cdot \nabla \times \vec{n} \propto \theta_0$). Furthermore, LC configurations that embed TDs exhibit reduced symmetry relative to the bulk nematic, and also have biaxial TD cores²³. Such nematic configurations might be visualized as a competition between helices exhibiting different directions, which can support an effective chirality^{18,22}. Thus, the combination of induced chirality and ion flow, both arising from the EHD instability, provide the necessary conditions for the corevolutions.

We now present experimental evidence that the co-revolution of the defects is related to the EHD instability. To examine this issue, we first measured the fields for the onset of the stationary EHD instability (E_{EHD1}) and the larger fields for the onset of mobility of the associated stripes (E_{EHD2}). These measurements were made at a location far from the TDs. Figure 8 shows a field vs. frequency "phase diagram", which combines the behaviours of the defect corevolution and the hydrodynamic instability. Data were collected at the four frequencies $\boldsymbol{\nu}$ of the applied field and the points were connected simply by straight line segments. The uniform red area, which appears as dark gray in monochrome at low fields, corresponds to $E < E_{rev1}$ for the defect co-revolution, viz., the defects are stationary. The yellow region, which appears as light gray in monochrome, corresponds to either pure wobble or mixed wobble/co-revolution, the latter represented by the overlap of the yellow (light gray) and dotted regions. At the highest fields, the dotted region over the white background represents the pure corevolution regime. Turning to the EHD instability, the stationary instability sets in at a field E_{EHD1} and the mobile instability at E_{EHD2} .

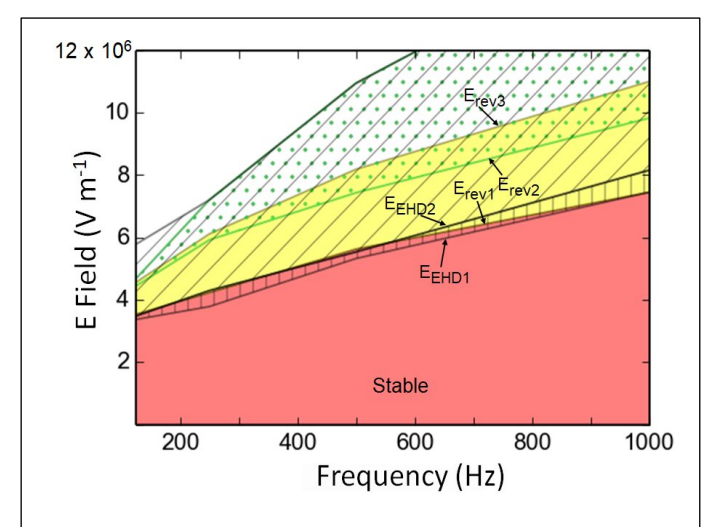


Fig. 8 Frequency / electric field "phase diagram" showing the various behaviours. See text for details. Note that the white region in the upper left part of the diagram corresponds to ill-defined turbulent behaviour.

The small region of stationary stripes occurs at fields $E_{EHD1} < E < E_{EHD2}$ and is represented by vertical lines. The mobile stripe regime, where $E > E_{EHD2}$, is shown by diagonal lines. It is quite apparent from Fig. 8 that wobble of the TDs occurs at nearly the same field E_{rev1} as the onset E_{EHD1} of the stationary EHD instability or the onset E_{EHD2} of the mobile instability. Although this holds true at all four frequencies, it is unclear which of E_{EHD1} or E_{EHD2} is the relevant field due to

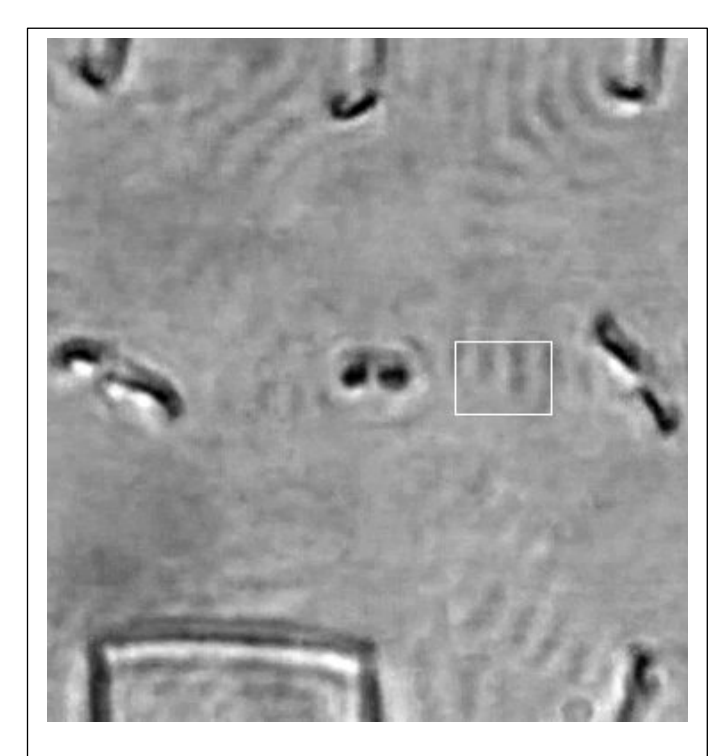


Fig. 9 Microscope image of the defects and the EHD instability. Here v = 250 Hz and $\it E$ = 5.6 x 10^6 V m $^{-1}$. At a given time and for a given x-coordinate, the average intensity is calculated along the y-axis inside the white box shown. The result is plotted in Fig. 10. The horizontal width of the white box corresponds to 10 μm . [Note the disclination line in the lower left, which unlike the other defects discussed in the work, lie parallel to the cell plane of the cell. Ref. 24]

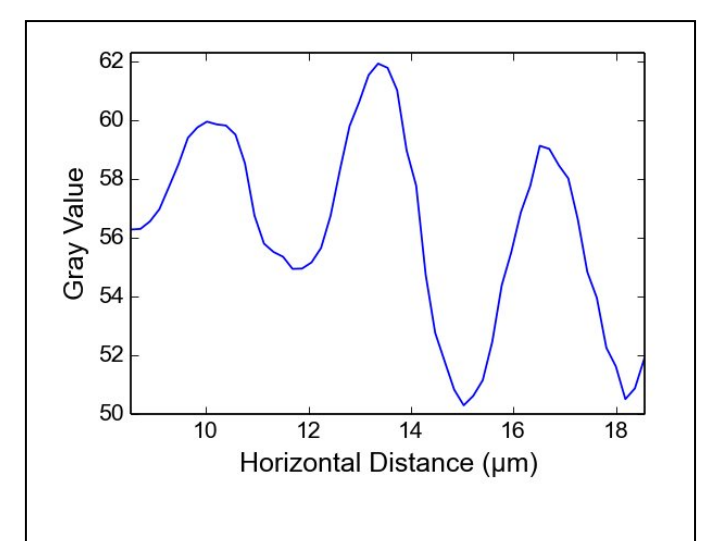


Fig. 10 Average intensity along the x-axis inside the white box in Fig. 9, with $\, v = 250 \, \text{Hz}$ and $E = 5.6 \times 10^6 \, \text{V m}^{-1}$. For $E > E_{EHD2}$, the profile translates to the left in each successive time frame, facilitating a determination of the velocity and the temporal period P_{EHD} . Note that the shape of the curve does not remain uniform in time, but evolves slowly relative to the temporal period.

experimental uncertainty in measuring the field and that the EHD instability thresholds were measured away from the defects.

We then examined the temporal period P_{EHD} of the mobile EHD defects, which appear approximately as moving stripes. This measurement contains significant uncertainty, as the stripes would often split or merge as they move. Nevertheless, to quantify approximately their motion, we examined a video in the region of the defects as a function of frequency and voltage. Figure 9 shows a frame of the video, including the EHD stripes. For each position along the x-axis inside the white box, the intensity was averaged along the y-axis in the box, resulting in a plot of intensity vs. position along the x-axis (Fig. 10). This procedure was performed for each of the 300 video frames comprising the 10 s video at a fixed applied field E. The translation along the x-axis of the intensity extrema was then examined frame-by-frame, that is, as a function of time, from which a characteristic speed s of stripes was obtained (typically at a distance of $^{\sim}$ 15 μm from the centre of co-revolution). From the spatial separation L of the stripes we obtained an approximate temporal period $P_{EHD} = L/s$ for the stripes at an applied field E and frequency v. (This corresponds to the time required for one wavelength of the hydrodynamic instability to pass by a fixed observer.) Results for the inverse period, $1/P_{EHD}$, are plotted as squares in Fig. 5. As can be seen, the inverse temporal period $1/P_{EHD}$ of the EHD instability is comparable to $1/P_{wob}$ for the wobbling defects at all frequencies and over the relevant field range, i.e., E > E_{rev3} .

The phase diagram in Fig. 8 shows remarkable agreement between the threshold fields for the movement of the TDs and those of the EHD instability. Likewise, Fig. 5 indicates excellent agreement between the *inverse* temporal periods for both the stripes and the wobbling defects. (Unfortunately, the EHD data become very noisy at higher fields and cannot be compared sufficiently quantitatively to the co-revolution period.) Although not proof, these agreements would suggest that the co-revolution

Journal Name ARTICLE

of the topological defects is not a stand-alone phenomenon. Rather, it likely is driven by the presence of the Carr-Helfrich EHD instability. At lower applied fields the magnitude of the instability is below a threshold required to supply sufficient force to drive a complete revolution of the defects, resulting in defect wobble. Looked at another way, the patterned substrate is able to trap the pair of m =+½ surface defects close to their equilibrium positions. At larger fields, the qualitative appearance of the EHD instability remains the same, although the optical contrast is found to increase - this indicates a larger amplitude — and the temporal period P_{EHD} decreases. (That is, the inverse temporal period $1/P_{EHD}$ increases.) In this region where $E > E_{rev2}$ the surface TDs became mobile at the patterned substrate and (at least) intermittent co-revolution can occur. Moreover, there is a concomitant decrease in the period P_{wob} of the wobbling defects, which follows P_{EHD} , as noted above. We note that there is little change in the qualitative appearance of the $% \left(1\right) =\left(1\right) \left(1$ EHD stripes as the field is increased above E_{rev2} , where co-revolution first appears. Thus, it seems clear that the co-revolution of the defects is induced by the EHD instability. At this point the intricate details that couple the two phenomena still need to be fully elucidated.

There currently is a significant effort in "active" materials, and "active nematics" are no exception²⁵⁻²⁸. Typically, adenosine triphosphate (ATP) is hydrolysed to power clusters of kinesin motors attached to microtubules — these are the structural units of the lyotropic nematic LC — resulting in mechanical stresses that drive the attendant motion. Might the co-revolving TDs also be considered an "active" nematic? This may be a matter semantics, although there is a clear distinction between the two systems. The classical active nematic is powered by a source of chemical energy that continues to drive the system until the ATP is depleted on its own; in general, it cannot be switched off by an external agent. The co-revolution phenomenon reported here is apparently driven by an external electric field through an intermediate electrohydrodynamic The co-revolution would, in principle, continue indefinitely until the external field is switched off by an external agent. This distinction leads us to conclude that the co-revolution should not be considered as an active nematic system in the classical sense.

4 Conclusions

We have shown that an electric field can drive azimuthal motion in a pair of antipodal $m=\pm \frac{1}{2}$ topological defects. That this phenomenon occurs only in a negative dielectric anisotropy liquid crystal suggests that it may be linked to an extension of the well-known Carr-Helfrich type electrohydrodynamic instability. As functions of amplitude and frequency of the electric field, optical measurements show remarkable agreement between these two phenomena, both in their threshold behaviours and their temporal periods. Thus, the electric field-driven co-revolution of ordinarily static topological defects appears to be mediated by the EHD instability — possibly the associated domain and ion flow, as well as the induced chiral symmetry in the LC — resulting in an electro

Lehmann-like effect. Work is underway to explicate theoretically this phenomenon.

Conflicts of interest

There are no conflicts to declare.

Acknowledgments

CR thanks Prof. Hillel Aharoni for useful discussions, and the Weizmann Institute of Science, Rehovot, Israel for a Weston Visiting Professorship. This work was supported financially by the National Science Foundation under grant DMR1901797 and by the National Aeronautics and Space Administration under grant NNX17AC76G and the Slovenian Research Agency (ARRS) under contracts P1-0099 and PR-07585.

Notes and references

- 1 N. Mermin, Rev. Mod. Phys., 1979, **51**, 591
- 2 W. H. Zurek, Nature, 1985, 317, 505
- 3 Y. Zhenwei and M.O. Cruz, Proc. Nat. Acad. Sci., 2014, 111, 5049
- 4 T.W.B. Kibble, J. Phys. A Math Gen., 1976, 9, 1387
- 5 A. Martinez, M. Ravnik, B. Lucerno, R. Visvanathan, S. Žumer, and I.I. Smaylyukh, *Nature Mater.*, 2014, **13**, 258
- 6 M. Kleman and O.D. Lavrentovich, Soft Matter Physics, Springer-Verlag, New York 2003
- 7 F. Serra, Liq. Cryst., 2016, **43**, 1920
- S. Zhou, S.V. Shiyanovskii, H.-S. Park, and O.D. Lavrentovich, Nature Comm., 2017, 8, 14974 (DOI: 10.1038/ncomms14974)
- 9 B.S. Murray, S. Kralj, and C. Rosenblatt, *Soft Matter*, 2017, **13**, 8442
- 10 A.J. Ferris, S. Afghah, R.L.B. Selinger, J.V. Selinger, and C. Rosenblatt, Soft Matter, 2020, 16, 642
- 11 A.L. Susser, S. Harkai, S. Kralj, and C. Rosenblatt, *Soft Matter*, 2020, **16**, 4814
- 12 C. Chiccoli, I. Feruli, O. D. Lavrentovich, P. Pasini, S. V. Shiyanovskii and C. Zannoni, *Phys. Rev. E: Stat., Nonlinear, Soft Matter Phys.*, 2002, **66**, 030701
- 13 E.F. Carr, J. Chem. Phys. 1963, 38, 1536
- 14 E.F. Carr, Mol. Cryst. Liq. Cryst. 1969, 7, 253
- 15 W. Helfrich, J. Chem. Phys., 1969, **51**, 4092
- 16 See S. Chandrasekhar, **Liquid Crystals**, CambridgeU. Press, 1993
- 17 P. Oswald and A. Dequid, Liq. Cryst., 2009, 36, 1071
- 18 H. R. Brand, H. Pleiner, and D. Svensek, Phys. Rev. E, 2013, 88, 024501
- 19 B. S. Murray, R. A. Pelcovits and C. Rosenblatt, *Phys. Rev. E: Stat., Nonlinear, Soft Matter Phys.*, 2014, **90**, 052501
- 20 I.M. Syed, G. Carbone, C. Rosenblatt, and Bing Wen, J. Appl. Phys. 2005, 98, 034303
- 21 S.J. DeCamp, G.S. Redner, A. Baskaran, M.F. Hagan, and Z. Dogic, *Nature Mat.*, 2015, **14**, 1110
- 22 L. G. Fel, Phys. Rev. E, 1995, 52, 702
- 23 N. Schopohl and T. J. Sluckin, *Phys. Rev. Lett.* 1987, **59**, 2582
- 24 S. Harkai, B.S. Murray, C. Rosenblatt, and S. Kralj, *Phys. Rev. Research*, 2020, **2**, 013176

- 25 Orsay Liquid Crystal Group, Mol. Cryst. Liq. Cryst., 1971, 12, 251
- 26 M.M. Norton, A. Baskaran, A. Opathalage, B. Langeslay, S. Fraden, A. Baskaran, and M.F. Hagan, *Phys. Rev. E*, 2018, 97, 012702
- 27 O. Pathalage, M.M. Norton, M.P.N. Juniper, B. Langelsay, S.A. Aghvami, and S. Fraden, *Proc. Nat. Acad. Sci.*, 2019, **116**, 4788
- 28 M.M. Norton, P. Grover, M.F. Hagan, and S. Fraden, *Phys. Rev. Lett.*, 2020, **125** 178005